Inorganica Chimica Acta 561 (2024) 121871

Contents lists available at ScienceDirect

Inorganica Chimica Acta

journal homepage: www.elsevier.com/locate/ica

Co/Mn-based 2D coordination polymers: synthesis, structure and ring opening polymerization

Yi Gong, Timothy J. Prior, Carl Redshaw *

Chemistry, School of Natural Sciences, University of Hull, Hull HU6 7RX, UK

ARTICLE INFO

Keywords:
2D coordination polymers
Ring opening polymerization
ε-caprolactone
δ-valerolactone

ABSTRACT

The two-dimensional coordination polymers $[Co(DMF)_2L_2]\bullet 0.65H_2O$ and $[Mn(DMF)_2L_2]\bullet 0.4H_2O$ (L = *N*,*N*′-bis(glycinyl)pyromellitic diimide) have been prepared and structurally characterized by a variety of techniques including FTIR spectroscopy, powder and single crystal X-ray diffraction. Results for their use as catalysts in the ring opening polymerization of ε-caprolactone (ε-CL) and δ-valerolactone (δ-VL) are reported. High conversions were achievable at 130 °C, resulting in the formation of mostly cyclic polycaprolactone (PCL) and polyvalerolactone (PVL), respectively, with only a small number of linear polymers formed. Kinetic studies revealed the presence of two distinct rate steps, the second of which is assigned to the formation of an active decomposition product.

1. Introduction

Two-dimensional coordination polymers (CPs) have exhibited excellent performance in the field of catalysis [1–4]. Such structures may also be referred to as two-dimensional metal–organic frameworks (2D MOFs) or two-dimensional metal–organic layers (MOLs) [5,6]. Besides the high surface activity characteristic commonly found in most 2D materials, CPs also possess specific and adjustable chemical functionalities as an added advantage [7]. By deliberate selection and synthesis of organic ligands, researchers can tailor CPs to meet specific application requirements. One example is the synthesis of two Cd-based CPs by Kumar and Paul using a novel organic ligand containing *N*- and *O*-donor functional groups [8]. These CPs exhibited outstanding properties for dye adsorption and desorption as well as catalysis. In addition, the coordination bonds in CPs are reversible, allowing for flexible interactions between the ligands and metal ions and even self-assembly [7–11]. It should be noted that the catalytic activity of metal–organic frameworks (MOFs) is often influenced by the constraints imposed by their framework structure [12]. However, the 2D structure of CPs can mitigate the impact of framework constraints.

Ring opening polymerization (ROP) is a common method for synthesizing eco-friendly and biodegradable polymers, such as polycaprolactone (PCL) and polyvalerolactone (PVL) [13,14]. Typically, the process is catalysed by a transition metal catalyst in the form of an alkoxide [M−OR] [15], though rare-earth metal [16], main group [17] and organic catalysts [18] can also be employed. Recent studies have also shown that the use of multinuclear metals systems can be beneficial [19], whilst the use of external stimuli for ROP is an emerging area [20]. Moreover, structure/activity relationships for ROP remain a key topic coupled with the search for the rate determining transition states [21].

CPs are a type of hybrid materials composed of organic linkers and inorganic metal ions, which can be classified as heterogeneous catalysts with superior performance and recyclability compared to homogeneous catalysts [22]. Many metal–organic complexes have been utilized as catalysts for ROP, exhibiting remarkable catalytic activity [23–26]. CPs and MOFs, similar to metal–organic complexes, possess metal active sites and organic linkers. Additionally, CPs and MOFs are ideal options for catalysts due to their large specific surface area and abundance of metal active sites.

Considering that there is limited research on the application of CPs or MOFs as catalysts in ROP, we employed *N*,*N*′-bis(glycinyl)pyromellitic diimide (LH_2, Fig. 1) as our entry point in order to synthesize two CPs $[Co(DMF)_2L_2]\bullet 0.65H_2O$ (referred as Co-L) and $[Mn(DMF)_2L_2]\bullet 0.4H_2O$ (referred as Mn-L) and have investigated their ROP potential. Both systems were capable of high conversions at elevated temperatures and exhibited two different catalytic mechanisms, the second of which were ascribe to an active decomposition product. The polymerization products formed via ROP were mostly cyclic in nature.

Interestingly, while this manuscript was in preparation, Liu *et al.* also reported a 1D cobalt-based polymer, the synthesis of which utilized L

* Corresponding author.
E-mail address: C.Redshaw@hull.ac.uk (C. Redshaw).

https://doi.org/10.1016/j.ica.2023.121871
Received 1 October 2023; Received in revised form 4 November 2023; Accepted 25 November 2023
Available online 28 November 2023

Fig. 1. Structure of LH_2.

(and 2,7-di(4H-1,2,4-triazol-4yl)benzo[*lmn*] [3,8] phenanthroline-1,3,6,8-(2H,7H)-tetraone/DMF). However, in this case LH_2 decomposed to the anion 2,5-dicarboxyterephthalate and did not bind to the metal [27].

2. Method

2.1. General

Acetic acid, methanol, 1,2,4,5-benzenetetracarboxylic anhydride and glycine were purchased from Fisher Scientific. Dimethylformamide and ε-caprolactone were purchased from Alfa Aesar. Cobalt(II) nitrate hexahydrate, manganese(II) nitrate tetrahydrate and δ-valerolactone were purchased from Sigma-Aldrich. All reagents were used without further purification. The hydrothermal reactions proceeded in a temperature-controlled oven (Memmert UF 30PLUS). Catalysts were dried in a vacuum oven (50℃, overnight) prior to the ROP reaction. Infra-red (IR) data were collected using a Nicolet iS5 FTIR spectrometer with iD1 Transmission Diamond ATR. Elemental analyses were performed in the School of Natural Sciences (Chemistry) at the University of Hull. MALDI-TOF mass spectra were collected on a Bruker Maxis Impact HD Mass spectrometer in ESI positive mode. Thermogravimetric analysis (TGA) results were recorded on a PerkinElmer TGA 4000 thermogravimetric analyser under ambient atmosphere from 30 to 757 °C. Powder X-ray diffraction (PXRD) patterns were obtained using a PANAlytical Empyrean Series 2 powder diffractometer with a copper X-ray tube. ^{1}H NMR spectra were obtained on a JEOL ECZ 400S spectrometer operating at a frequency of 400.2 MHz. Gel Permeation Chromotography (GPC) tests were conducted using SHIMADZU liquid chromatography (LC-6A), Viscotek VE 3580 RI detector, Viscotek VE 5111 injector valve bracket, Viscotek 270 dual detector. The molecular weights and polydispersity index were determined by analyzing the experimental traces with the software OmniSEC 5.12.

2.2. Synthesis of L

The synthesis of *N,N′*-bis(glycinyl)pyromellitic diimide (LH_2) followed the previously reported literature method [28]. Benzene-1,2,4,5-tetracarboxylic dianhydride (1.09 g, 5 mmol) in 30 mL of acetic acid was heated to 40 °C. Then glycine (0.75 g, 10 mmol) was added, and the system was refluxed for 4 h. The reaction mixture was concentrated under reduced pressure, yielding LH_2 as a white powder (1.49 g, 90 % yield). NMR and FTIR spectroscopic results were in good agreement with the literature (Fig. S1 and Fig. 3(c)).

2.3. Synthesis of Co-L

Co-L was prepared by the following hydrothermal reaction: Co$(NO_3)_2{\cdot}6H_2O$ (0.145 g, 0.5 mmol) and LH_2 (0.166 g, 0.5 mmol) were added to 10 mL DMF. The resulting mixture was transferred into a 25 mL Telflon-lined autoclave, which was sealed and placed in a temperature-controlled oven at 120 ℃ for 18 h. The autoclave was allowed to cool down gradually to room temperature at a rate of 1℃ per hour, resulting in the formation of red rod-like shaped crystals. The obtained crystals were then decanted and dried in a vacuum oven. Yield: 72 %. Elem. anal. (%) for $C_{20}H_{20}CoN_4O_{10}$ Calcd: C 44.87, H 3.77, N 10.47; Found: C 45.44, H 3.56, N 10.67.

2.4. Synthesis of Mn-L

Mn-L was prepared as for Co-L but using $Mn(NO_3)_2{\cdot}4H_2O$ (0.125 g, 0.5 mmol) and L (0.166 g (0.5 mmol) affording Mn-L as yellow needle shaped crystals. Yield: 81 %. Elem. anal. (%) for $C_{20}H_{20}MnN_4O_{10}$ Calcd: C 45.21, H 3.79, N 10.54; Found: C 45.00, H 4.31, N 10.93.

2.5. Crystal structure determinations

Suitable crystals of Co-L and Mn-L were selected, and each was mounted on a Rigaku Oxford Diffraction Synergy Custom system, HyPix diffractometer. The crystal was kept at 100.00(10) K during data collection. Standard data collection and processing procedures were employed. Using Olex2 [29], the structure was solved with the SHELXT [30] structure solution program using Intrinsic Phasing and refined with the SHELXL [31] refinement package using Least Squares minimisation. Hydrogen atoms were placed using a riding model. In each structure there was a small region of unmodelled electron density away from the CP framework. This was modelled using a solvent mask with Olex2; small amounts of unbound, disordered, water were located within each structure.

Crystal Data for $C_{20}H_{20}CoN_4O_{10}$ ($M = 535.33$ g/mol): triclinic, space group *P*-1 (no. 2), $a = 9.6513(4)$ Å, $b = 10.1479(3)$ Å, $c = 13.5546(4)$ Å, $\alpha = 85.002(2)°$, $\beta = 71.920(3)°$, $\gamma = 63.319(3)°$, $V = 1125.48(8)$ Å^3, $Z = 2$, $T = 100.00(10)$ K, μ(Cu Kα) = 6.565 mm^{-1}, $Dcalc = 1.580$ g/cm^3, 48,475 reflections measured ($6.872° \leq 2\theta \leq 140.136$), 4201 unique ($R_{int} = 0.0685$, $R_{sigma} = 0.0274$) which were used in all calculations. The final R_1 was 0.0526 (I > 2 σ(I)) and wR_2 was 0.1696 (all data).

Crystal Data for $C_{20}H_{16}N_4O_{10}Mn$ ($M = 527.31$ g/mol): triclinic, space group *P*-1 (no. 2), $a = 9.8488(5)$ Å, $b = 10.0737(5)$ Å, $c = 13.5449(7)$ Å, $\alpha = 84.235(4)°$, $\beta = 71.370(4)°$, $\gamma = 64.089(5)°$, $V = 1144.21(11)$ Å^3, $Z = 2$, $T = 100.00(10)$ K, μ(Cu Kα) = 5.268 mm^{-1}, $Dcalc = 1.531$ g/cm^3, 21,605 reflections measured ($6.894° \leq 2\theta \leq 150.12$), 4599 unique ($R_{int} = 0.0334$, $R_{sigma} = 0.0203$) which were used in all calculations. The final R_1 was 0.0374 (I > 2 σ(I)) and wR_2 was 0.1193 (all data).

CCDC 2,298,025 and 2,298,026 contain the supplementary crystallographic data for this paper. These data can be obtained free of charge from the Cambridge Crystallographic Data Centre via https://www.ccdc.cam.ac.uk/structures.

2.6. ROP of ε-Caprolactone and δ-valerolactone

Polymerization of ε-CL or δ-VL was carried out using Co-L and Mn-L as catalysts under ambient atmosphere (melt). Catalyst and monomer were weighed out into a flask and the reaction mixture was then placed in a preheated oil bath at the desired temperature, followed by quenching using glacial acetic acid (0.2 mL) and cold methanol (10 mL). The reaction conversion was monitored using ^{1}H NMR spectroscopy (400 MHz, $CDCl_3$, 298 K), and the resulting polymer was collected after vaporization and dried in a fume hood. The polymers were then dissolved in CH_2Cl_2 and precipitated with cold methanol. Molecular weights (M_n and Đ) of the polymer products were determined using GPC in THF. Recycled catalysts were separated by dissolving the polymerization product in chloroform and centrifugation.

2.7. Kinetics studies

Kinetic experiments were conducted using the aforementioned

polymerization protocol. At suitable intervals, ~0.05 mL reagents were withdrawn, quenched with cold $CDCl_3$ (1 mL), and subjected to ^1H NMR spectroscopic analysis (400 MHz, $CDCl_3$, 298 K).

3. Results and discussion

3.1. Structures of Co-L and Mn-L

The structures of Co-L and Mn-L, as determined by single-crystal X-ray diffraction, are shown in Fig. 2a–d. These are isostructural and each crystallises in the triclinic space group *P*-1. Each metal in Co-L and Mn-L exhibits an octahedral coordination geometry. Each carboxylate group binds to two metals in bridging bidentate mode and four unique oxygen atoms bind to each metal in a square plane. All C···O distances of the carboxylates are roughly equal; the electron density is delocalised rather than being formally O═C − O$^-$. This produces chains of edge-sharing square planes that run parallel to the crystallographic *a* axis. The remaining two coordination sites on each metal are occupied by two *trans* DMF molecules. The two carboxylates at different ends of the ligand are bound in adjacent chains. The cross linking of the chains by the ligand gives rise to the 2-D sheet in the *xz* plane. Fig. 2e,f present the 2D layered structures of Co-L and Mn-L. Critically there are no strong intermolecular forces between the layer. It appears that there are only van der Waals interactions between layers. There is some additional electron density contained in channels running parallel to the *a*-axis corresponding to around 6 % of the cell volume. This was modelled using a solvent mask to give overall compositions $Mn(DMF)_2L_2{\cdot}0.4H_2O$ and $Co(DMF)_2L_2{\cdot}0.65H_2O$; it is notable that the C═O from the ligands project in these small channels, and there is the potential for hydrogen bonding between water and framework.

Fig. 3a,b demonstrate the good agreement between the experimental and simulated PXRD patterns of Co-L and Mn-L, confirming the purity and crystallinity of the synthesized bulk compounds. Fig. 3c presents the IR spectra of L, Co-L and Mn-L, respectively. The small peaks around 3000 cm^{-1} corresponding to the stretching vibrations of the C—H bonds. In the spectrum of L, sharp peaks at 2390–2290 cm^{-1} are attributed to the stretching vibrations of the O—H bonds in the carboxyl motif. Weak and broad peaks are observed in the spectra of Co-L and Mn-L due to a small quantity of carboxyl groups retained at the termini. Additionally, the peaks at 1812–1482 cm^{-1} correspond to the stretching vibrations of C═O bonds. The four split peaks in the spectra of Co-L and Mn-L can be attributed to C═O bonds in L and DMF. The peaks at 1167–982 cm^{-1} are characteristic of the C—N bonds in L.

3.2. Ring opening polymerization studies

Ring opening polymerization (ROP) of ε-caprolactone (ε-CL) and δ-valerolactone (δ-VL) were initiated by Co-L and Mn-L using different ratios of catalyst to monomer (1 to 100, 500, 1000). All reactions conducted at ambient atmosphere exhibited no activity when performed either under nitrogen or in the presence of solvent (toluene). According to Tables 1 and 2, the optimal [Cat]:[monomer] ratio for the ROP of ε-CL and δ-VL was found to be 1:500, affording high conversion (e.g. conversion = 98 %, Table 2, entry 5) and narrow polydispersity index (*e.g.* Đ = 1.34, Table 1, entry 5). With regard to the temperature, the majority of the catalysts only exhibited activity at 130℃, whilst only for the ROP of δ-VL initiated by Co-L was activity observed at 100℃ (Table 2, entry 7). End group analysis of the resulting polymers (Figs S3–S6) revealed that the dominant products were cyclic PCL and PVL, with only a small amount of linear polymers formed. In the MALDI-TOF mass spectra (Fig. 4), signal peaks at *m/z* 1053.6 (n = 9) and 3463.0 (n = 30) were assigned to cyclic PCL with Na^+ (*m/z*: 114.1 x n + 23.0) and cyclic PCL with K^+ (*m/z*: 114.1 x n + 39.1). Other peaks at *m/z* 1083.7 (n = 9), 3591.5 (n = 30), 3808.5 (n = 31) and 3921.1 (n = 34) corresponded to the quenching products with methanol and acetic acid, indicating the presence of linear PCL ($OH(CL)_nH$ with K^+ (*m/z*: 18.0 + 114.1 × n + 39.1), linear PCL ($OH(CL)_nH$ or $H_3CO(CL)_nH$) with Na^+ (*m/z*: 18.0 or 32.0 + 114.1 × n + 23.0). Uniformly distributed signal peaks at *m/z* 3942.9 (n = 39), 4043.3 (n = 40), 4143.7 (n = 41), 4244.0 (n = 42), 4344.3 (n = 43) and 4444.6 (n = 44) in the MALDI-TOF mass spectrum of PVL (Fig. 4c) were assigned to cyclic PVL with K^+ (*m/z*: 100.1 x n + 39.1). Signal peak at 1458.5 (n = 14) in Fig. 4d corresponded to the linear PVL ($OH(VL)_nH$ with K^+ (*m/z*: 18.0 + 100.1 × n + 39.1). The lower molecular weights (M_n) *versus* theoretical values suggest the occurrence of undesired transesterification processes during the ROP.

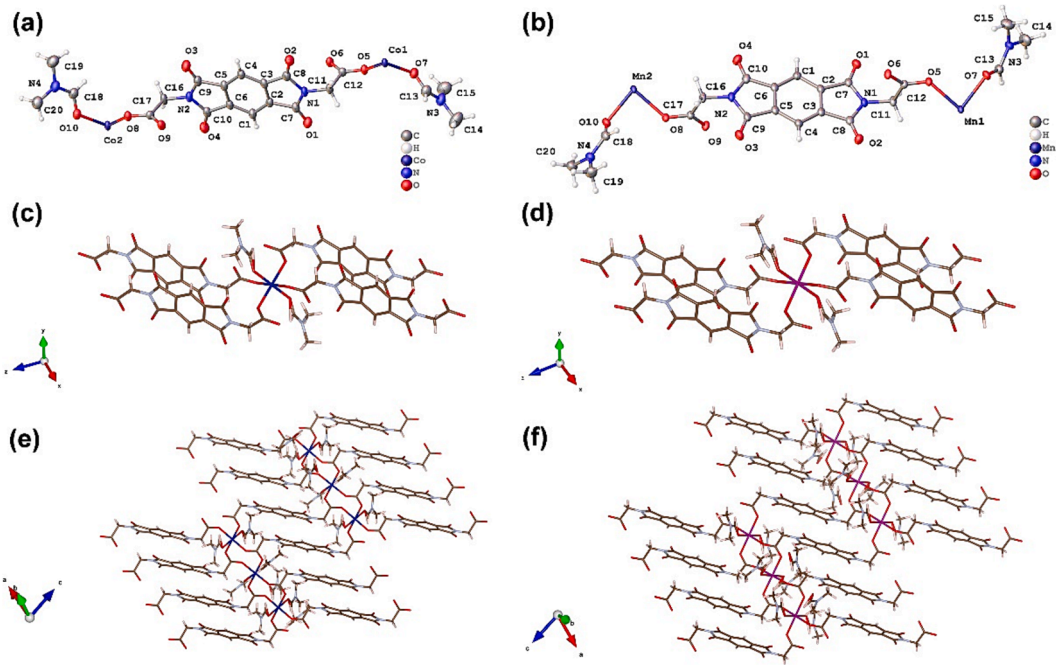

Fig. 2. Molecular structure of (a) Co-L and (b) Mn-L; Coordination environment of the central metal ion for (c) Co-L and (d) Mn-L; 2D layer structure of (e) Co-L and (f) Mn-L.

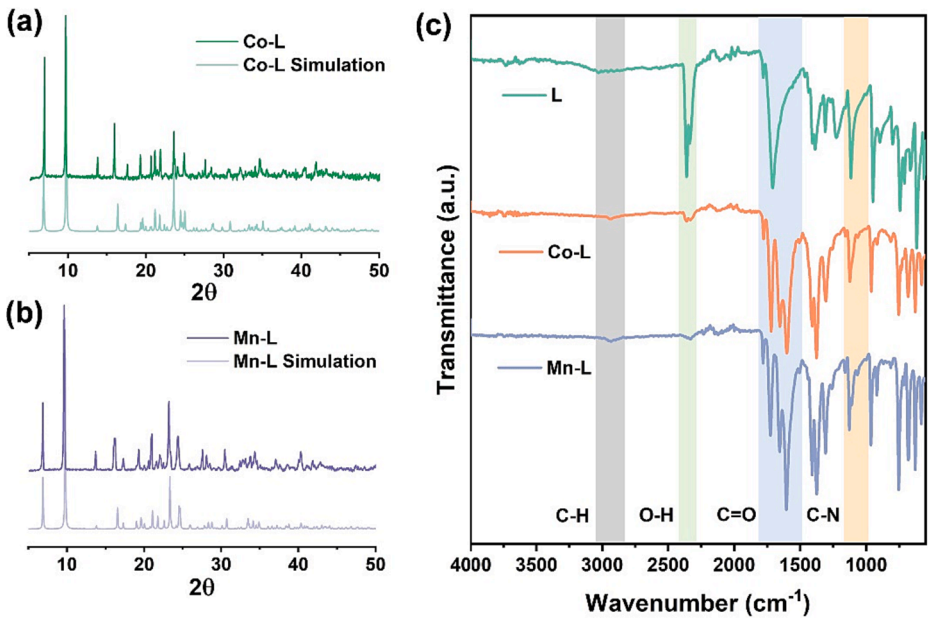

Fig. 3. Experimental and simulated X-ray powder diffraction patterns of (a) Co-L and (b) Mn-L; (c) Infrared spectra of L, Co-L, Mn-L.

Table 1
ROP of ε-CL initiated by Co-L and Mn-L under air as melts.

Entry	Catalyst	[Cat]:[CL]	Temp. (°C)	Conv. (%)[a]	M_n (*Da*)[b]	Đ [c]
1	Co-L	1:100	130	68	1010	2.24
2	Co-L	1:500	130	92	4490	1.77
3	Co-L	1:1000	130	39	4670	1.31
4	Mn-L	1:100	130	45	1200	2.34
5	Mn-L	1:500	130	90	7200	1.34
6	Mn-L	1:1000	130	82	3640	1.65
7	Co-L	1:500	100	–	–	–
8	Mn-L	1:500	100	–	–	–

Reaction conditions: 0.01 mmol of catalyst was used in each reaction, [Cat]:[CL] = 1:100, 1:500, 1:1000, 20 h. [a] Conversion was confirmed by ^{1}H NMR spectroscopy. [b] GPC analysis in THF at ambient temperature, the results were calibrated with polystyrene standards and corrected by a factor [32] of 0.56. [c] Polydispersity index (M_w/M_n) were calculated by GPC.

Table 2
ROP of δ-VL initiated by Co-L and Mn-L under air as melts.

Entry	Catalyst	[Cat]:[VL]	Temp. (°C)	Conv. (%)[a]	M_n (*Da*)[b]	Đ [c]
1	Co-L	1:100	130	87	4310	1.64
2	Co-L	1:500	130	95	5520	1.61
3	Co-L	1:1000	130	67	4740	1.23
4	Mn-L	1:100	130	75	1810	2.77
5	Mn-L	1:500	130	98	5640	2.24
6	Mn-L	1:1000	130	94	5250	1.80
7	Co-L	1:500	100	46	4180	1.36
8	Mn-L	1:500	100	–	–	–

Reaction conditions: 0.01 mmol of catalyst was used in each reaction, [Cat]:[VL] = 1:100, 1:500, 1:1000, 8 h. [a] Conversion was confirmed by ^{1}H NMR spectroscopy. [b] GPC analysis in THF at ambient temperature, the results were calibrated with polystyrene standards and corrected by a factor [32] of 0.57. [c] Polydispersity index (M_w/M_n) were calculated by GPC.

3.3. Kinetics studies

Kinetics studies using ε-CL or δ-VL catalyzed by Co-L and Mn-L were performed under air in the melt state (solvent-free). The ratio of monomer to catalyst utilized was 500 to 1. At certain time intervals (2 h for ε-CL; 1 h for δ-VL), a tiny amount of the reaction mixture was quenched in glacial $CDCl_3$ solution, and the conversion was determined by ^{1}H NMR spectroscopy. Fig. 5 illustrates the plot of time *vs* $\ln([CL]_0/[CL]_t)$ and $\ln([VL]_0/[VL]_t)$, and two clear slopes are evident. The two distinct rates corresponding to the two separate stages (denoted by blue and yellow). It can be clearly seen that the rate in the final stage is markedly faster than the one in the preceding stage. As shown in Fig. 5, the initial period for the ε-CL systems (12–14 h) was somewhat longer than that observed for δ-VL (3 h). In the subsequent second stage, the ROP of ε-CL with Co-L proceeded at a slow rate from 4 h to 12 h (Fig. 5a). In the case of Mn-L, the ROP of ε-CL with Mn-L exhibited a higher rate than Co-L over 4 to 14 h (Fig. 5b), whilst in the second stage, the rate involving Co-L is slightly faster than that of Mn-L. As indicated by Fig. 4c,d, the rate of ROP with δ-VL involving Co-L in both stages is marginally faster than that involving Mn-L.

When we isolated the catalysts post ROP, we compared their FTIR spectra and PXRD with that of the pre-ROP species. For example, the spectra for the Co-L system are provided in Fig. S7, SI. There were clear differences in both the FTIR and PXRD indicating that the nature of the catalyst had changed. Given this, in a separate experiment, we heated up the catalyst alone to the temperature employed for the ROP process (*i.e.* 130 °C), and on cooling re-recorded the FTIR spectra and PXRD. Again, the FTIR spectra and PXRD had changed and were exactly as we found post-ROP. We therefore infer that during the ROP process the catalyst 'decomposes' into a second active species. On-going studies, such as attempting to grow single crystals of this 'decomposition' product will help to identify the nature of this product and will be reported separately. We note that for the ROP of lactide catalysed by $Zn(C_6F_5)_2$/Lewis base, a bifunctional activation mechanism has been proposed [33].

4. Conclusion

In summary, two 2D coordination polymers, Co-L and Mn-L, have been synthesized and their molecular structures determined using single crystal X-ray diffraction studies, as well as PXRD, IR spectroscopy and elemental analyses. These 2D structures have been utilized for the ROP of ε-caprolactone (ε-CL) and δ-valerolactone (δ-VL), and at elevated temperatures (130 °C), favourable results in terms of conversion and polydispersity index were achieved. The majority of the polymers produced consisted of cyclic products, as identified by NMR spectroscopy and MALDI-TOF mass spectra. Two distinct steps were observed in the kinetics studies, the second of which is assigned to an active 'decomposition' product. The Co-based system was found to exhibit a slightly

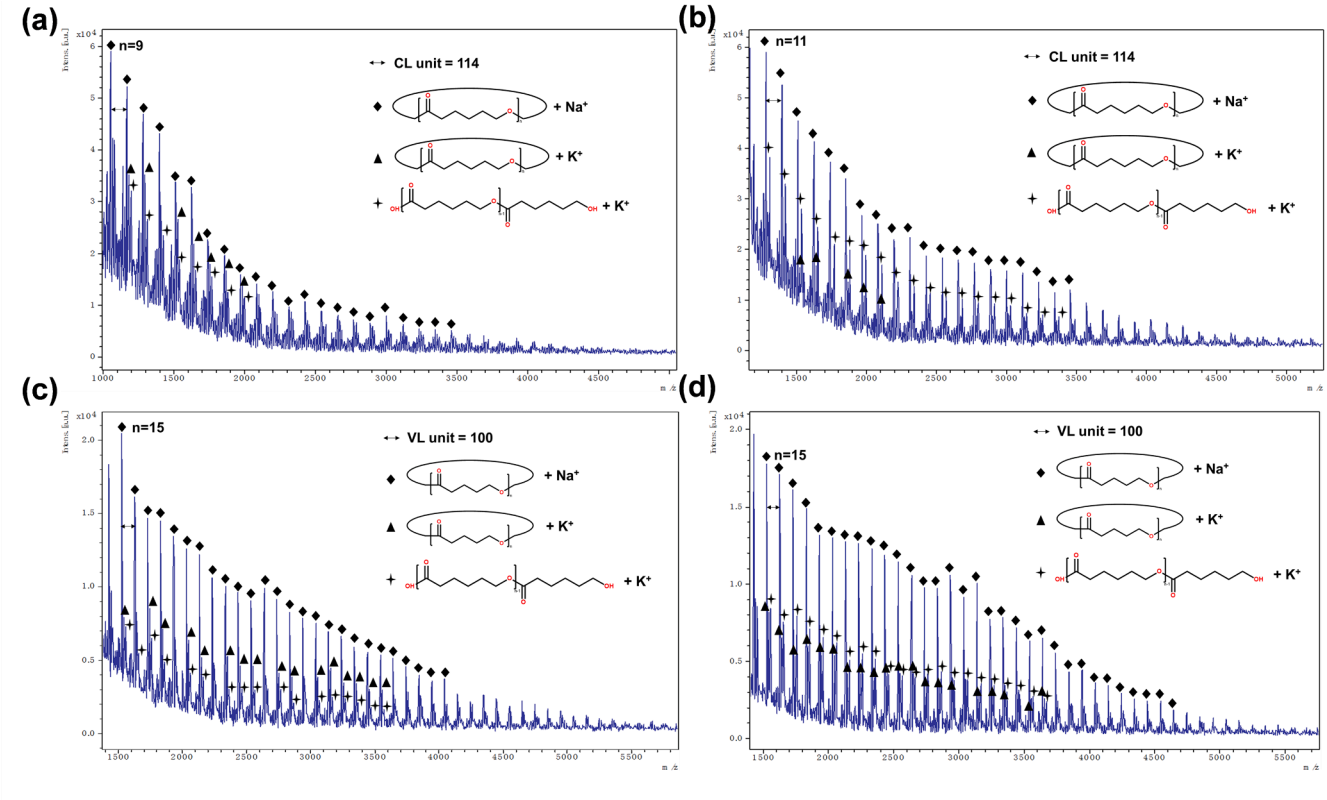

Fig. 4. MALDI-TOF mass spectrum of (a) PCL (Table 1, entry 2), (b) PCL (Table 1, entry 5), (c) PVL (Table 2, entry 2) and (d) PVL (Table 2, entry 5).

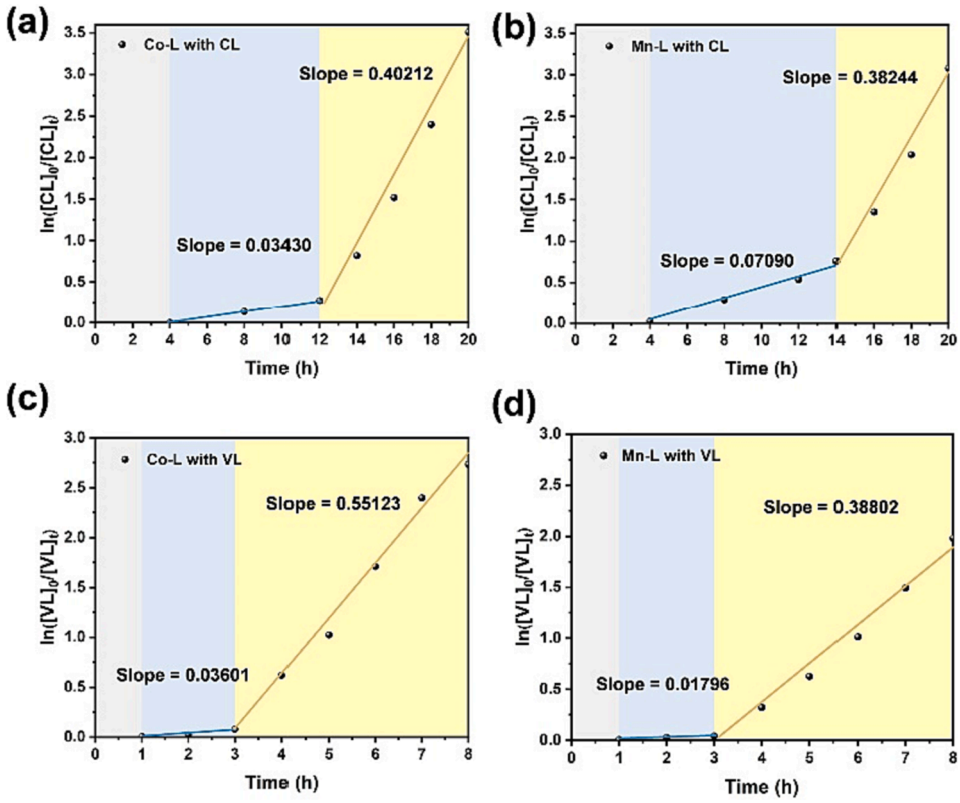

Fig. 5. Plot of $\ln([CL]_0/[CL]_t)$ *vs.* time for the polymerization of ε-CL initiated by (a) Co-L and (b) Mn-L at ratio of catalyst to monomer = 1: 500; Plot of $\ln([VL]_0/[VL]_t)$ *vs.* time for the polymerization of δ-VL initiated by (c) Co-L and (d) Mn-L at ratio of catalyst to monomer = 1: 500.

faster kinetic profile than the Mn-based system. Further studies are in process to identify the nature of the active 'decomposition' catalyst.

CRediT authorship contribution statement

Yi Gong: Investigation, Writing – review & editing. **Timothy J. Prior:** Investigation. **Carl Redshaw:** Funding acquisition, Supervision, Writing – review & editing.

Declaration of competing interest

The authors declare that they have no known competing financial interests or personal relationships that could have appeared to influence the work reported in this paper.

Data availability

Data will be made available on request.

Acknowledgements

The China Scholarship Council (CSC) is thanked for supporting Yi Gong. Dean Moore (UoH) is thanked for help with data collection. CR thanks the EPSRC for funding (grant no. EP/S025537/1) and the UK National Crystallographic Service at Southampton for data collection.

Appendix A. Supplementary data

Supplementary data to this article can be found online at https://doi.org/10.1016/j.ica.2023.121871.

References

[1] L. Tom, M.R.P. Kurup, A 2D-layered Cd(II) MOF as an efficient heterogeneous catalyst for the Knoevenagel reaction, J. Solid State Chem. 294 (2021), 121846, https://doi.org/10.1016/j.jssc.2020.121846.
[2] P. Li, W. Liu, J.S. Dennis, H.C. Zeng, Ultrafine alloy nanoparticles converted from 2d intercalated coordination polymers for catalytic application, Adv. Funct. Mater. 26 (2016) 5658–5668, https://doi.org/10.1002/adfm.201601174.
[3] A.M. Kirillov, Y.Y. Karabach, M.V. Kirillova, M. Haukka, A.J.L. Pombeiro, Topologically Unique Heterometallic CuII/Mg Coordination Polymer: Synthesis, Structural Features, and Catalytic Use in Alkane Hydrocarboxylation 12 (2012) 1069–1074, https://doi.org/10.1021/cg201459k.
[4] S. Zhou, G. Yan, B. Gao, W. Jiang, B. Liu, T. Zhou, C. Liu, G. Che, A layered Mn-based coordination polymer as an efficient heterogeneous catalyst for CO2 cycloaddition under mild conditions, CrystEngComm. 24 (2022) 4527–4533, https://doi.org/10.1039/d2ce00579d.
[5] A. Dhakshinamoorthy, A.M. Asiri, H. Garcia, 2D Metal-Organic Frameworks as Multifunctional Materials in Heterogeneous Catalysis and Electro/Photocatalysis, Adv. Mater. 31 (2019), https://doi.org/10.1002/adma.201900617.
[6] L. Cao, T. Wang, C. Wang, Synthetic Strategies for Constructing Two-Dimensional Metal-Organic Layers (MOLs): A Tutorial Review, Chinese J. Chem. 36 (2018) 754–764, https://doi.org/10.1002/cjoc.201800144.
[7] M. Tran, K. Kline, Y. Qin, Y. Shen, M.D. Green, S. Tongay, 2D coordination polymers: Design guidelines and materials perspective, Appl. Phys. Rev. 6 (2019), https://doi.org/10.1063/1.5110895.
[8] N. Kumar, A.K. Paul, Triggering Lewis Acidic Nature through the Variation of Coordination Environment of Cd-Centers in 2D-Coordination Polymers, Inorg. Chem. 59 (2020) 1284–1294, https://doi.org/10.1021/acs.inorgchem.9b02997.
[9] S. Wang, H. Xing, Y. Li, J. Bai, Y. Pan, M. Scheer, X. You, 2D and 3D cadmium(II) coordination polymers from a flexible tripodal ligand of 1,3,5-tris(carboxymethoxy)benzene and bidentate pyridyl-containing ligands with three-, eight- and ten-connected topologies, Eur. J. Inorg. Chem. (2006) 3041–3053, https://doi.org/10.1002/ejic.200600189.
[10] W. Yang, X. Lin, A.J. Blake, C. Wilson, P. Hubberstey, N.R. Champness, M. Schröder, Self-assembly of metal-organic coordination polymers constructed from a bent dicarboxylate ligand: Diversity of coordination modes, structures, and gas adsorption, Inorg. Chem. 48 (2009) 11067–11078, https://doi.org/10.1021/ic901429u.
[11] H. Kajiro, A. Kondo, K. Kaneko, H. Kanoh, Flexible two-dimensional square-grid coordination polymers: Structures and functions, Int. J. Mol. Sci. 11 (2010) 3803–3845, https://doi.org/10.3390/ijms11103803.
[12] L. Cao, Z. Lin, F. Peng, W. Wang, R. Huang, C. Wang, J. Yan, J. Liang, Z. Zhang, T. Zhang, L. Long, J. Sun, W. Lin, Self-Supporting Metal-Organic Layers as Single-Site Solid Catalysts, Angew. Chemie - Int. Ed. 55 (2016) 4962–4966, https://doi.org/10.1002/anie.201512054.
[13] O. Nuyken, S.D. Pask, Ring-opening polymerization-An introductory review, Polymers (basel). 5 (2013) 361–403, https://doi.org/10.3390/polym5020361.
[14] S. Penczek, J. Pretula, S. Slomkowski, Ring-Opening Polymerization 3 (2021) 33–57, https://doi.org/10.1515/cti-2020-0028.
[15] A. Arbaoui, C. Redshaw, Metal caltalysts for ε-caprolactone polymerisation, Polym. Chem. 1 (2010) 801–826, https://doi.org/10.1039/B9PY00334G.
[16] D.M. Lyubov, A.O. Tolpygin, A.A. Trifonov, Rare-earth metal complexes as catalysts for ring-opening polymerization of cyclic esters, Coord. Chem. Rev. 392 (2019) 83, https://doi.org/10.1016/j.ccr.2019.04.013.
[17] E. Fazekas, P.A. Lowy, M.A. Rahman, A. Lykkeberg, Y. Zhou, R. Chambenahalli, J. A. Garden, Main group metal polymerization catalysts, Chem. Soc. Rev. 51 (2022) 8793–8814, https://doi.org/10.1039/D2CS00048B.
[18] A.P. Dove, Organic catalysis for ring-opening polymerization, ACS Macro Lett. 1 (2012) 1409–1412, https://doi.org/10.1021/mz3005956.
[19] L.-J. Wu, W. Lee, P.K. Ganta, Y.-L. Chang, Y.-C. Chang, H.-Y. Chen, Multinuclear metal catalysts in ring-opening polymerization of ε-caprolactone and lactide: Cooperative and electronic effects between metal centers, Coord. Chem. Rev. 475 (2023), 214847, https://doi.org/10.1016/j.ccr.2022.214847.
[20] S. Kaler, M.D. Jones, Recent advances in externally controlled ring-opening polymerisations, Dalton Trans. 51 (2022) 1241–1256, https://doi.org/10.1039/D1DT03471E.
[21] W.-H. Rao, L. Yu, J.-D. Ding, Stride Strategy to Enable a Quasi-ergodic Search of Reaction Pathways Demonstrated by Ring-opening Polymerization of Cyclic Esters. Chin, J. Polym. Sci. 41 (2023) 745–759, https://doi.org/10.1007/s10118-023-2930-6.
[22] T.A. Goetjen, J. Liu, Y. Wu, J. Sui, X. Zhang, J.T. Hupp, O.K. Farha, Metal-organic framework (MOF) materials as polymerization catalysts: A review and recent advances, Chem. Commun. 56 (2020) 10409–10418, https://doi.org/10.1039/d0cc03790g.
[23] W. Gruszka, A. Lykkeberg, G.S. Nichol, M.P. Shaver, A. Buchard, J.A. Garden, Combining alkali metals and zinc to harness heterometallic cooperativity in cyclic ester ring-opening polymerisation, Chem. Sci. 11 (2020) 11785–11790, https://doi.org/10.1039/d0sc04705h.
[24] P. Brignou, S.M. Guillaume, T. Roisnel, D. Bourissou, J.F. Carpentier, Discrete cationic zinc and magnesium complexes for dual organic/organometallic-catalyzed ring-opening polymerization of trimethylene carbonate, Chem. - A Eur. J. 18 (2012) 9360–9370, https://doi.org/10.1002/chem.201200336.
[25] W.T. Diment, G.L. Gregory, R.W.F. Kerr, A. Phanopoulos, A. Buchard, C. K. Williams, Catalytic Synergy Using Al(III) and Group 1 Metals to Accelerate Epoxide and Anhydride Ring-Opening Copolymerizations, ACS Catal. 11 (2021) 12532–12542, https://doi.org/10.1021/acscatal.1c04020.
[26] F.J. Lai, T.W. Huang, Y.L. Chang, H.Y. Chang, W.Y. Lu, S. Ding, H.Y. Chen, C. C. Chiu, K.H. Wu, Titanium complexes bearing 2,6-Bis(o-hydroxyalkyl)pyridine ligands in the ring-opening polymerization of L-Lactide and ε-caprolactone, Polymer (guildf). 204 (2020), 122860, https://doi.org/10.1016/j.polymer.2020.122860.
[27] D. Shen, Y. Sha, C. Chen, X. Chen, Q. Jiang, H. Liu, W. Liu, Q. Liu, A one-dimensional cobalt-based coordination polymer as a cathode material of lithium-ion batteries, Dalt. Trans. 52 (2023) 7079–7087, https://doi.org/10.1039/d3dt00398a.
[28] N. Barooah, R.J. Sarma, J.B. Baruah, Solid-state hydrogen bonded assembly of N, N′-bis(glycinyl)- pyromellitic diimide with aromatic guests, CrystEngComm. 8 (2006) 608–615, https://doi.org/10.1039/b607323a.
[29] O.V. Dolomanov, L.J. Bourhis, R.J. Gildea, J.A.K. Howard, H. Puschmann, OLEX2: A complete structure solution, refinement and analysis program, J. Appl. Crystallogr. 42 (2009) 339–341, https://doi.org/10.1107/S0021889808042726.
[30] G.M. Sheldrick, SHELXT - Integrated space-group and crystal-structure determination, Acta Crystallogr. Sect. A Found. Crystallogr. 71 (2015) 3–8, https://doi.org/10.1107/S2053273314026370.
[31] G.M. Sheldrick, Crystal structure refinement with SHELXL, Acta Crystallogr. Sect. C, Struct. Chem. 71 (2015) 3–8, https://doi.org/10.1107/S2053229614024218.
[32] M. Save, A. Soum, Controlled ring-opening polymerization of lactones and lactide initiated by lanthanum isopropoxide, 2a: Mechanistic studies, Macromol. Chem. Phys. 203 (2002) 2591–2603, https://doi.org/10.1002/macp.200290043.
[33] X.Q. Li, B. Wang, H.Y. Ji, Y.S. Li, Insights into the mechanism for ring-opening polymerization of lactide catalyzed by Zn(C6F5)2/organic superbase Lewis pairs, Catal, Sci. Technol. 6 (2016) 7763–7772, https://doi.org/10.1039/c6cy01587e.